Advances in Nano Research, *Vol. 13, No.5 (2022) 427-435*
https://doi.org/10.12989/anr.2022.13.5.427

Nonlinear static behavior of three-layer annular plates reinforced with nanoparticles

Shouhua Liu[1], Jikun Yu*[2], H. Elhosiny Ali[3,4,5] and Murtadha M. Al-Masoudy[6]

[1]*College of Architectural Engineering, Huaiyin Institute of Technology, Huaian 223021, Jiangsu, China*
[2]*Institute of Applied Technology, Dalian Ocean University, Dalian 116000, Liaoning, China*
[3]*Advanced Functional Materials & Optoelectronic Laboratory (AFMOL), Department of Physics, Faculty of Science, King Khalid University, P.O. Box 9004, Abha 61413, Saudi Arabia*
[4]*Research Center for Advanced Materials Science (RCAMS), King Khalid University, P.O. Box 9004, Abha 61413, Saudi Arabia*
[5]*Physics Department, Faculty of Science, Zagazig University, Zagazig 44519, Egypt*
[6]*Air conditioning and refrigeration Technique Engineering Department, Al-Mustaqbal University College, Babylon 51001, Iraq*

(*Received June 26, 2021, Revised January 24, 2022, Accepted June 15, 2022*)

Abstract. Static stability behaviors of annular sandwich plates constructed from two layers of particle-reinforced nano-composites have been investigated in the present article. The type of nanoscale particles has been considered to be graphene oxide powders (GOPs). The particles are assumed to have uniform and graded dispersions inside the matrix and the material properties have been defined according to Halpin-Tsai micromechanical model. The core layer is assumed to have honeycomb configuration. Annular plate has been formulated according to thin shell assumptions considering geometrical nonlinearities. After solving the governing equations via Galerkin's technique, it is showed that the post-buckling curves of annular sandwich plates rely on the core wall thickness, amount of GOP particles, sector radius, and thickness of layers.
Keywords: annular plate; graphene oxide powder; nanoparticles; nonlinear stability; post-buckling

1. Introduction

Based on recent developments, a variety of carbon based structures containing carbon nanotube or carbon fiber have been widely utilized in composites for enhancing their mechanics and thermal specifications (Liu *et al*. 2008, Zhang 2017, Xiong *et al*. 2020, Mirjavadi *et al*. 2021). A 273% enhancement of elastic modulus is obtained by Ahankari *et al*. (2010) for carbon reinforced composites in comparison to conventional composites. Likewise, Gojny *et al*. (2004) mentioned that structural stiffness of carbon based composites may be enhanced with incorporation of carbon nanotube within material. Impacts of configuration and scale of carbon nanotubes on rigidity growth of material composites having metallic matrices are studied by Esawi *et al*. (2011). Because of representing above cited properties, beam and plate structures fortified by small scale fillers have been investigated to determine their static or dynamical properties (Barati and Shahverdi 2017a, b, Yang *et al*. 2017, Mirjavadi *et al*. 2022). There are also some researches on composites and other reinforced materials and interested scholars are referred to the recent researches (Barati 2017a, b, Barati and Zenkour 2018, 2019, Al-Maliki *et al*. 2019, Wu *et al*. 2021, Ebrahimi and Barati 2019a, b, Ebrahimi *et al*. 2019, Mirjavadi *et al*. 2020a, b, c, d, e). In addition, the graphene filled composite material has been recently gained enormous attentions because of representing easy producing procedure and high rigidity growth. Nieto *et al*. (2017) presented a review paper based on several graphene based composite material possessing ceramic or metallic matrices. The multi-scale study of mechanical attributes for graphene based composite material has been provided by Lin *et al*. (2018) utilizing finite elements approach.

Until now, many of researches in the fields of nano-composites have been interested in production and materials characteristics recognition of graphene based composites and structural components containing slight percentages of graphene fillers. For instance, it is mentioned by Rafiee *et al*. (2009) that some material characteristics of graphene based composites may be enhanced via placing 0.1% volume of graphene filler. However, achieving to this level of reinforcement employing nanotubes required 1% of their volume. Graphene based composites containing epoxy matrix were created by King *et al*. (2013) by placing 6% weight fraction of graphene fillers to polymeric phases. It was stated that Young modulus of the composite has been increased from 2.72 GPa to 3.36 GPa. Next, 57% increment for Young modulus has been achieved by Fang *et al*. (2009) based on a sample of graphene based composite.

Moreover, many studies in the fields of nano-mechanic (Ebrahimi and Brati 2017a, b, c, d, e, 2018a, b, c, d, e, f) are associated with vibrational and stability investigation of various structural elements containing beam or plate reinforced via diverse graphene dispersions. For instance, vibrational properties of a laminated graphene based plate have been explored by Song *et al*. (2017) assuming simply support edge condition. They assumed that the plate is constructed from particular numbers of layers each

*Corresponding author, Ph.D.,
E-mail: yujikun@dlou.edu.cn

ISSN: 2287-237X (Print), 2287-2388 (Online)

containing a sensible content of graphene. Selecting a perturbation approach, static deflections and bucking loads of graphene based plates have been derived by Shen *et al*. (2017). In above papers, each material property has discontinuous variation across the thickness of beam or plate. Also, geometrically nonlinear vibration frequencies of graphene based beams having embedded graphene have been explored by Feng *et al*. (2017) selecting first-order beam theory. Moreover, vibration frequencies of graphene based beams having porosities have been explored by Kitipornchai *et al*. (2017).

Furthermore, reinforcement of matrix materials with nano-size inclusions is a novel case study (Guenaneche *et al*. 2019, Zaheer *et al*. 2019, Guan *et al*. 2020). Many researches show that mechanical properties of concrete can be enhanced by adding graphene platelets (GPLs), graphene oxide powders (GOPs) and ever carbon nanotubes (Du *et al*. 2016, Shamsaei *et al*. 2018). Graphene oxide, as derivative of graphene, is broadly and economically available from graphite mass oxidations. It is compatible with many matix materials including polymeric materials and even concrete (Mohammed *et al*. 2017). Graphene oxide composite exhibits great Young modulus and tensile strength as are carbon-based material with remarkable performances and low costs (Zhang *et al*. 2020). To the best of author's knowledge, post-buckling study of geometrically imperfect (Wang *et al*. 2018) annular sector plates reinforced by nanoparticles is not carried out till to now.

In the present article, static stability behaviors of annular sandwich plates constructed from two layers of particle-reinforced nanocomposites have been investigated. The type of nanoscale particles has been considered to be graphene oxide powders (GOPs). The particles are assumed to have uniform and graded dispersions inside the matrix and the material properties have been defined according to Halpin-Tsai micromechanical model. The core layer is assumed to have honeycomb configuration. Annular plate has been formulated according to thin shell assumptions considering geometrical nonlinearities. After solving the governing equations via Galerkin's technique, it is exhibited that the post-buckling curves of annular sandwich plates rely on the core wall thickness, amount of GOP particles, sector radius, and thickness of layers.

2. GOP particle reinforced composites

In this research, the type of nanoscale particles has been considered to be graphene oxide powders (GOPs). An annular sandwich plate with GOP-reinforced layers and honeycomb core has been shown in Fig. 1. Micro-mechanic theory of such composite materials (Liew *et al*. 2015) introduces the below relationship between nanoparticles weight fraction ($W_{particle}$) and their volume fraction ($V_{particle}$) by:

$$\boldsymbol{V^*_{particle}} = \frac{\boldsymbol{W_{particle}}}{\boldsymbol{W_{particle}} + \frac{\boldsymbol{\rho_{particle}}}{\boldsymbol{\rho_M}} - \frac{\boldsymbol{\rho_{particle}}}{\boldsymbol{\rho_M}}\boldsymbol{W_{particle}}} \quad (1)$$

where $\rho_{particle}$ and ρ_M define the mass densities of nano-particle and matrices, respectively. Next, the elastic modulus

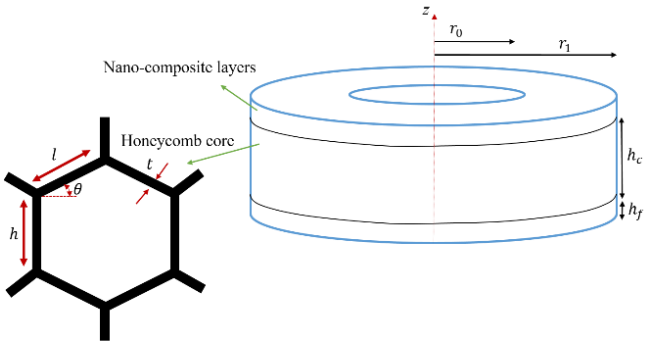

Fig. 1 Configuration of the annular sandwich plate

of a nanoparticle based composite might be represented based upon matrix elastic modulus (E_M) by (Zhang *et al*. 2020):

$$\boldsymbol{E_1} = \boldsymbol{0.49}\left(\frac{\boldsymbol{1+\xi_L^{particle}\eta_L^{particle}V_{particle}}}{\boldsymbol{1-\eta_L^{particle}V_{particle}}}\right)\boldsymbol{E_M} + \boldsymbol{0.51}\left(\frac{\boldsymbol{1+\xi_W^{particle}\eta_W^{particle}V_{particle}}}{\boldsymbol{1-\eta_W^{particle}V_{particle}}}\right)\boldsymbol{E_M} \quad (2)$$

so that $\xi_L^{particle}$ and $\xi_W^{particle}$ define two geometrical factors indicating the impacts of nanoparticle configuration and scales as:

$$\xi_L^{particle} = \frac{2d_{particle}}{t_{particle}} \quad (3a)$$

$$\eta_L^{particle} = \frac{\left(E_{particle}/E_M\right)-1}{\left(E_{particle}/E_M\right)+\xi_L^{particle}} \quad (3b)$$

$$\xi_W^{particle} = \frac{2d_{particle}}{t_{particle}} \quad (3c)$$

$$\eta_W^{particle} = \frac{\left(E_{particle}/E_M\right)-1}{\left(E_{particle}/E_M\right)+\xi_W^{particle}} \quad (3d)$$

so that $d_{particle}$ and $t_{particle}$ define nanoparticle average diameter and thickness, respectively. Furthermore, Poisson's ratio for nanoparticle based composite might be defined based upon Poisson's ratio of the two constituents in the form:

$$v_1 = v_{particle}V_{particle} + v_M V_M \quad (4a)$$

in which $V_M = 1 - V_{particle}$ expresses the volume fractions of matrix component (Metwally *et al*. 2014). Herein, three dispersions of the nanoparticle have been assumed as:

$$V_{particle} = \begin{cases} V^*_{particle} & \text{(UD)} \\ 2V^*_{particle}\left(1-\frac{2|z|}{h}\right) & \text{(FG-O)} \\ 4V^*_{particle}\frac{|z|}{h} & \text{(FG-X)} \end{cases} \quad (4b)$$

3. Modeling of honeycomb cores

It must be stated that honeycomb cores can be replaced

by solid cores having the same material characteristics (Barati and Shahverdi 2022). The configuration of honeycomb cells has been illustrated in Fig.1. According to Gibson model, the solid core has below material properties as:

$$\boldsymbol{E_c = E_s\left(\frac{t}{l}\right)^3 \frac{cos(\theta)}{(h/l + sin(\theta))\, sin^2(\theta)} \frac{1}{1 + cot^2(\theta)\,(t/l)^2}} \quad (5a)$$

$$\boldsymbol{v_c = \frac{cos^2(\theta)}{(h/l + sin(\theta))\, sin(\theta)} \frac{1 - (t/l)^2}{1 + cot^2(\theta)\,(t/l)^2}} \quad (5b)$$

$$\boldsymbol{G_c = E_s\left(\frac{t}{l}\right)^3 \frac{(h/l + sin(\theta))}{(h/l)^2\, cos(\theta)} \frac{1}{R}}$$
$$\boldsymbol{R = \begin{pmatrix} 1 + 2\frac{h}{l} + \left(\frac{t}{l}\right)^2 \frac{h/l + sin(\theta)}{(h/l)^2} \\ * \left[(h/l + sin(\theta))\, tan^2(\theta) + sin(\theta)\right] \end{pmatrix}} \quad (5c)$$

in which E_c is Young modulus in *x* direction; v_c denotes Poison's ratio and G_c is the in-plane shear modulus. Moreover, E_s denotes the Young's modulus of constituent material which is Aluminum in the present paper. The symbols *t*, *h*, *l* have been displayed in Fig. 1, however, *t* denotes the cell wall thickness; *h* and *l* denote the cell dimensions. It must be stated that for a regular honeycomb core which has isotropic properties, *h*/*l*=1 and $\theta = \pi/6$. According to the above explanations, a honeycomb core sandwich plate may be considered as a solid core sandwich plate displayed in Fig. 1.

4. Derivation of equations of motion

Considering inner radius (r_0), outer radius (r_1) and sector angel (ψ), Fig.1 illustrates the geometry of an annular sector plate. As mentioned, the annular sector is made of nanoparticle reinforced composite material for which the stresses σ_p (p=r, φ, $r\varphi$) can be determined as:

$$\begin{Bmatrix} \sigma_r \\ \sigma_\varphi \\ \sigma_{r\varphi} \end{Bmatrix} = \begin{pmatrix} Q_{11} & Q_{12} & 0 \\ Q_{12} & Q_{22} & 0 \\ 0 & 0 & Q_{66} \end{pmatrix} \begin{Bmatrix} \varepsilon_r \\ \varepsilon_\varphi \\ \gamma_{r\varphi} \end{Bmatrix} \quad (6)$$

in which

$$Q_{11} = Q_{22} = \frac{E_1}{1 - v_1^2},$$
$$Q_{12} = \frac{v_1 E_1}{1 - v_1^2}, Q_{66} = \frac{E_1}{2(1 + v_1)} \quad (7)$$

The same relations are applicable for honeycomb cores. For a thin annular sector plate, components of strain field considering nonlinear deflection are (Barati and Zenkour 2019):

$$\varepsilon_r = \varepsilon_r^0 - z\chi_r,$$
$$\varepsilon_\varphi = \varepsilon_\varphi^0 - z\chi_\varphi,$$
$$\gamma_{r\varphi} = \gamma_{r\varphi}^0 - 2z\chi_{r\varphi} \quad (8)$$

in which

$$\varepsilon_r^0 = \frac{\partial u}{\partial r} + \frac{1}{2}\left(\frac{\partial w}{\partial r}\right)^2,$$
$$\varepsilon_\varphi^0 = \frac{1}{r}\left(\frac{\partial v}{\partial \varphi} + u\right) + \frac{1}{2r^2}\left(\frac{\partial w}{\partial \varphi}\right)^2, \quad (9)$$
$$\gamma_{r\varphi}^0 = \frac{\partial v}{\partial r} - \frac{v}{r} + \frac{1}{r}\frac{\partial u}{\partial \varphi} + \frac{1}{r}\frac{\partial w}{\partial r}\frac{\partial w}{\partial \varphi},$$
$$\chi_r = \frac{\partial^2 w}{\partial r^2}, \chi_\varphi = \frac{1}{r}\frac{\partial w}{\partial r} + \frac{1}{r^2}\frac{\partial^2 w}{\partial \varphi^2},$$
$$\chi_{r\varphi} = \frac{1}{r}\frac{\partial^2 w}{\partial r \partial \varphi} - \frac{1}{r^2}\frac{\partial w}{\partial \varphi}$$

Plate deflection is denoted by *w* and in-plane displacements are denoted by *u* and *v*. Annular sector plate contains stresses which result in below forces and moments via integrating Eq. (6) over sector thickness:

$$\begin{Bmatrix} N_r \\ N_\varphi \\ N_{r\varphi} \end{Bmatrix} = \begin{pmatrix} A_{11} & A_{12} & 0 \\ A_{12} & A_{22} & 0 \\ 0 & 0 & A_{66} \end{pmatrix} \begin{Bmatrix} \varepsilon_r^0 \\ \varepsilon_\varphi^0 \\ \gamma_{r\varphi}^0 \end{Bmatrix} - \begin{pmatrix} B_{11} & B_{12} & 0 \\ B_{12} & B_{22} & 0 \\ 0 & 0 & B_{66} \end{pmatrix} \begin{Bmatrix} \chi_r \\ \chi_\varphi \\ 2\chi_{r\varphi} \end{Bmatrix} \quad (10)$$

$$\begin{Bmatrix} M_r \\ M_\varphi \\ M_{r\varphi} \end{Bmatrix} = \begin{pmatrix} B_{11} & B_{12} & 0 \\ B_{12} & B_{22} & 0 \\ 0 & 0 & B_{66} \end{pmatrix} \begin{Bmatrix} \varepsilon_r^0 \\ \varepsilon_\varphi^0 \\ \gamma_{r\varphi}^0 \end{Bmatrix} - \begin{pmatrix} D_{11} & D_{12} & 0 \\ D_{12} & D_{22} & 0 \\ 0 & 0 & D_{66} \end{pmatrix} \begin{Bmatrix} \chi_r \\ \chi_\varphi \\ 2\chi_{r\varphi} \end{Bmatrix} \quad (11)$$

in which

$$A_s = \int_{-h_c/2-h_f}^{-h_c/2} Q_s^f\, dz + \int_{-h_c/2}^{h_c/2} Q_s^c\, dz + \int_{h_c/2}^{h_c/2+h_f} Q_s^f\, dz,$$
$$B_s = \int_{-h_c/2-h_f}^{-h_c/2} Q_s^f z\, dz + \int_{-h_c/2}^{h_c/2} Q_s^c z\, dz + \int_{h_c/2}^{h_c/2+h_f} Q_s^f z\, dz,$$
$$D_s = \int_{-h_c/2-h_f}^{-h_c/2} Q_s^f z^2\, dz + \int_{-h_c/2}^{h_c/2} Q_s^c z^2\, dz + \int_{h_c/2}^{h_c/2+h_f} Q_s^f z^2\, dz,$$
$$s = \{11,12,22,66\} \quad (12)$$

Finally, one may express the governing equations for an annular sector plate as:

$$\frac{\partial N_r}{\partial r} + \frac{1}{r}\frac{\partial N_{r\theta}}{\partial \theta} + \frac{1}{r}(N_r - N_\theta) = 0 \quad (13)$$

$$\frac{\partial N_{r\theta}}{\partial r} + \frac{1}{r}\frac{\partial N_\theta}{\partial \theta} + \frac{2}{r}N_{r\theta} = 0 \quad (14)$$

$$\frac{\partial^2 M_r}{\partial r^2} + \frac{2}{r}\frac{\partial M_r}{\partial r} + \frac{2}{r}\frac{\partial^2 M_{r\theta}}{\partial r \partial \theta} + \frac{2}{r^2}\frac{\partial M_{r\theta}}{\partial \theta} + \frac{1}{r^2}\frac{\partial^2 M_\theta}{\partial \theta^2} - \frac{1}{r}\frac{\partial M_\theta}{\partial r} + N_r\left(\frac{\partial^2 w}{\partial r^2}\right) - 2N_{r\theta}\left[\frac{1}{r^2}\left(\frac{\partial w}{\partial \theta}\right) - \frac{1}{r}\left(\frac{\partial^2 w}{\partial r \partial \theta}\right)\right] + N_\theta\left[\frac{1}{r}\left(\frac{\partial w}{\partial r}\right) + \frac{1}{r^2}\left(\frac{\partial^2 w}{\partial \theta^2}\right)\right] - P_r\left(\frac{\partial^2 w}{\partial r^2}\right) = 0 \quad (15)$$

where P_r is radial load. By substituting Eqs. (10)-(11) into Eqs. (13) and (15), nonlinear governing equations in terms

of strain components can be simply expressed in compact forms:

$$\begin{aligned}&\frac{\partial}{\partial r}[A_{11}\varepsilon_r^0+A_{12}\varepsilon_\varphi^0-B_{11}\chi_r-B_{21}\chi_\varphi]\\&+\frac{1}{r}\frac{\partial}{\partial\theta}[A_{66}\gamma_{r\varphi}^0-2B_{66}\chi_{r\varphi}]\\&+\frac{1}{r}(A_{11}\varepsilon_r^0+A_{12}\varepsilon_\varphi^0-B_{11}\chi_r-B_{21}\chi_\varphi\\&-A_{12}\varepsilon_r^0-A_{22}\varepsilon_\varphi^0+B_{12}\chi_r+B_{22}\chi_\varphi)=0\end{aligned}\tag{16}$$

$$\begin{aligned}&\frac{\partial}{\partial r}[A_{66}\gamma_{r\varphi}^0-2B_{66}\chi_{r\varphi}]\\&+\frac{1}{r}\frac{\partial}{\partial\theta}[A_{12}\varepsilon_r^0+A_{22}\varepsilon_\varphi^0-B_{12}\chi_r-B_{22}\chi_\varphi]\\&+\frac{2}{r}[+A_{66}\gamma_{r\varphi}^0-2B_{66}\chi_{r\varphi}]=0\end{aligned}\tag{17}$$

$$\begin{aligned}&(\frac{\partial^2}{\partial r^2}+\frac{2}{r}\frac{\partial}{\partial r})[B_{11}\varepsilon_r^0+B_{12}\varepsilon_\varphi^0-D_{11}\chi_r+D_{12}\chi_\varphi]\\&+(\frac{2}{r}\frac{\partial^2}{\partial r\partial\theta}+\frac{2}{r^2}\frac{\partial}{\partial\theta})[B_{66}\gamma_{r\varphi}^0-2D_{66}\chi_{r\varphi}]\\&+\frac{1}{r^2}\frac{\partial^2}{\partial\theta^2}[B_{12}\varepsilon_r^0+B_{22}\varepsilon_\varphi^0-D_{12}\chi_r-D_{22}\chi_\varphi]\\&-\frac{1}{r}\frac{\partial}{\partial r}[B_{12}\varepsilon_r^0+B_{22}\varepsilon_\varphi^0-D_{12}\chi_r-D_{22}\chi_\varphi]\\&+[A_{11}\varepsilon_r^0+A_{12}\varepsilon_\varphi^0-B_{11}\chi_r-B_{21}\chi_\varphi](\frac{\partial^2w}{\partial r^2})\\&-2[A_{66}\gamma_{r\varphi_r}^0-2B_{66}\chi_{r\varphi}][\frac{1}{r^2}(\frac{\partial w}{\partial\theta})-\frac{1}{r}(\frac{\partial^2w}{\partial r\partial\theta})]\\&+[A_{12}\varepsilon_r^0+A_{22}\varepsilon_\varphi^0-B_{12}\chi_r-B_{22}\chi_\varphi][\frac{1}{r}(\frac{\partial w}{\partial r})\\&+\frac{1}{r^2}(\frac{\partial^2w}{\partial\theta^2})]-P_r(\frac{\partial^2w}{\partial r^2})=0\end{aligned}\tag{18}$$

5. Method of solution

Presented in this chapter is numerical solution of the non-linear governing equations for post-buckling of a nanoparticle-reinforced annular sandwich plate. The below edge conditions may be introduced for mechanical post-buckling analyzes of simply-supported plate as:

$$\begin{aligned}&w=M_r=N_{r\theta}=0\ \text{ at r=r}_0\text{,r=r}_1\\&w=M_\theta=N_{r\theta}=0\ \text{ at }\theta=0,\psi\end{aligned}\tag{19}$$

According to the thin sector plate formulation, the displacement field may be selected as (Hao *et al*. 2022, Afshari *et al*. 2022):

$$u=\sum_{i=1}^{\infty}\sum_{j=1}^{\infty}U_{ij}(t)\frac{\partial H_i(r)}{\partial r}R_j(\varphi)\tag{20}$$

$$v=\sum_{i=1}^{\infty}\sum_{j=1}^{\infty}V_{ij}(t)H_i(r)\frac{\partial R_j(\varphi)}{\partial\varphi}\tag{21}$$

$$w\ =\sum_{i=1}^{\infty}\sum_{j=1}^{\infty}W_{ij}(t)H_i(r)\,R_j(\varphi)\tag{22}$$

where (U,V,W) are the displacements amplitudes; and the functions H_i and R_j are the test functions which are selected as:

$$H_i(r)=sin\frac{i\pi(r-r_0)}{r_1-r_0},\ R_j(\varphi)=sin\left(\frac{j\pi\varphi}{\psi}\right)\tag{23}$$

Arranging the governing equations as B_i (u, v, w, w^*)=0 with (i=1,2,3) and inserting field components presented as Eqs.(20)-(22) into B_i yields following equations with the use of Galerkin's technique:

$$\int_{r_0}^{r_1}\int_0^{\psi}B_1\frac{\partial H_i(r)}{\partial r}R_j(\varphi)rdrd\varphi=0\tag{24}$$

$$\int_{r_0}^{r_1}\int_0^{\psi}B_2\,H_i(r)\frac{\partial R_j(\varphi)}{\partial\varphi}rdrd\varphi=0\tag{25}$$

$$\int_{r_0}^{r_1}\int_0^{\psi}B_3\,H_i(r)R_j(\varphi)rdrd\varphi=0\tag{26}$$

After solving Eqs. (24)-(26) by neglecting in-plane inertias, three governing equations will be derived:

$$S_{11}U+S_{21}V+S_{31}W+H_1W^2=0\tag{27}$$

$$S_{12}U+S_{22}V+S_{32}W+H_2W^2=0\tag{28}$$

$$\begin{aligned}&S_{13}U+S_{23}V+S_{33}W+H_3W^2+H_4W^3\\&+H_5UW+H_6VW-P^*(W)=0\end{aligned}\tag{29}$$

in which S_{ij} are linear stiffness matrix components; H_i denotes nonlinear stiffness components and Y_i are added stiffness due to geometric imperfection. Also, P^* denote the geometric matrix related to applied load. With the aid of Eqs. (27)-(29) one can express that

$$\begin{aligned}U&=\frac{S_{21}S_{32}-S_{22}(S_{31})}{S_{11}S_{22}-S_{12}S_{21}}W+\frac{H_2S_{21}-H_1S_{22}}{S_{11}S_{22}-S_{12}S_{21}}W^2\\V&=\frac{S_{12}S_{31}-S_{11}(S_{32})}{S_{11}S_{22}-S_{12}S_{21}}W+\frac{H_1S_{12}-H_2S_{11}}{S_{11}S_{22}-S_{12}S_{21}}W^2\end{aligned}\tag{30}$$

Then, applying Eq. (30) in Eq. (29) yields a single equation based on W only. The numerical solution of obtained equation for finding P_r will give post-buckling curves.

6. Discussion on results

In this section, post-buckling of a particle-reinforced annular sector sandwich plate modeled via nonlinear thin shell theory has been studied based upon provided solution approach. The dependency of post-buckling load $\tilde{P}_r=P_r/10^6h$, on GOP particles, plate radius, normalized amplitude, honeycomb core and sector angle will be explored. In this research, the material properties of GOP particle reinforced annular plate are obtained when $d_{particle}=500\,nm,\ t_{particle}=0.95\,nm$. Also, Table 1 give the details of material properties for the matrix and GOP particles. As the first step, post-buckling responses of a plate have been validated with those reported by Chikh *et al*. (2016) based on functionally graded (FG) plate model, as provided in Table 2. According to the table, buckling loads have been provided based on various normalized amplitude.

Table 1 Material properties of the GOP particle reinforced composite

	Epoxy	GOP
E (GPa)	3.45	444.8
ν	0.35	0.165
ρ (kg/m^3)	1270	1090

Table 2 Comparison of post-buckling loads of a plate for various normalized amplitude

$\widetilde{W}/h$	Chikh *et al*. 2016	present
0	0.62411	0.62412
0.1	0.62627	0.62628
0.2	0.63274	0.63275
0.3	0.64354	0.64355

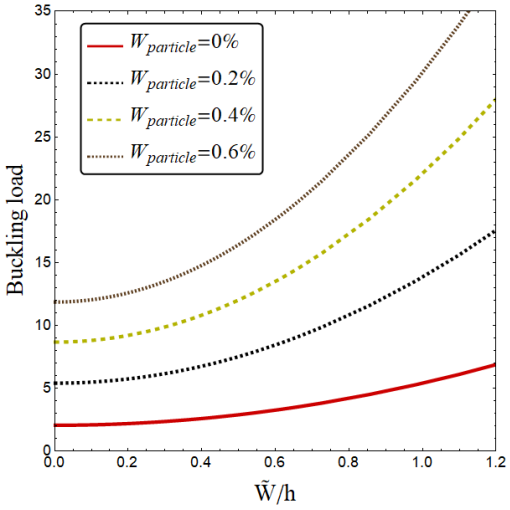

Fig. 2 Buckling load variation against non-dimensional amplitude of sandwich annular plate based on various particle weight fraction (h_f=0.2h, r_1=50h, r_0=0.2r_1, t=0.01l)

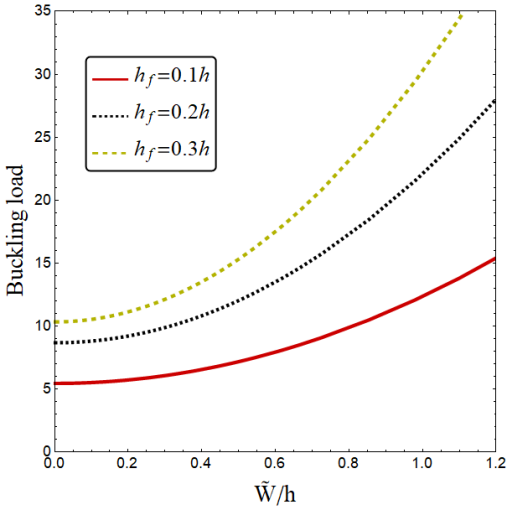

Fig. 3 Buckling load variation against non-dimensional amplitude of sandwich annular plate based on various thickness of layers ($W_{particle}$=0.4%, r_1=50h, r_0=0.2r_1, t=0.01l)

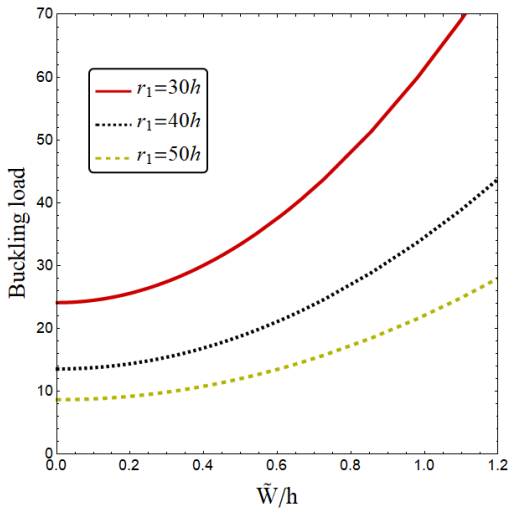

Fig. 4 Buckling load variation against non-dimensional amplitude of sandwich annular plate based on various plate radius ($W_{particle}$=0.4%, h_f=0.2h, r_0=0.2r_1, t=0.01l)

Effects of particle weight fraction ($W_{particle}$) on the buckling load variation of an annular sandwich plate have been illustrated in Fig. 2 when h_f=0.2h and r_1=50h. Uniform GOP particle dispersion has been assumed. It must be stated that, the buckling load when the non-dimensional amplitude is zero $\widetilde{W}/h = 0$, is critical buckling load. For non-zero values of non-dimensional amplitude, the buckling load values of higher and the annular plate is in the post-buckling state. In fact, with the growth of non-dimensional amplitude, the buckling load magnitude increases which means that the annular plate stiffness has been increased. Also, reinforcing influences of GOP particles on buckling properties of annular sandwich plate is apparently perceptible from the figure. Indeed, the equivalent stiffness of annular sandwich plates can be perceptibly strengthened by attaching a small content of GOP particles into the matrix phase. This means that increase of particle weight fraction in the layers of annular sandwich plate results in higher buckling loads.

In Fig. 3, the variation of buckling load versus non-dimensional amplitude of sandwich annular plate has been depicted according to various thickness for layers (h_f). For this figure, particle weight fraction of $W_{particle}$=0.4% in the layers with uniform dispersion has been assumed. It is evident from the figure that increase of layer's thickness leads to higher buckling loads. This is because higher values of layer's thickness are corresponding to higher total stiffness of the annular sandwich plate. In fact, the reason is due to the fact that particle reinforced layers have higher stiffness than the core.

Impacts of plate radius (r_1) on post-buckling properties of particle-reinforced annular sandwich plates have been exhibited in Fig. 4. It is evident from the figure that a particle-reinforced annular sandwich plate is less rigid at higher magnitudes of plate radius. Subsequently, the buckling load becomes smaller by the growth of plate radius at prescribed non-dimensional amplitudes ($\widetilde{W}/h$). As a conclusion, the annular sandwich plates is more flexible as it radius (r_1) becomes larger.

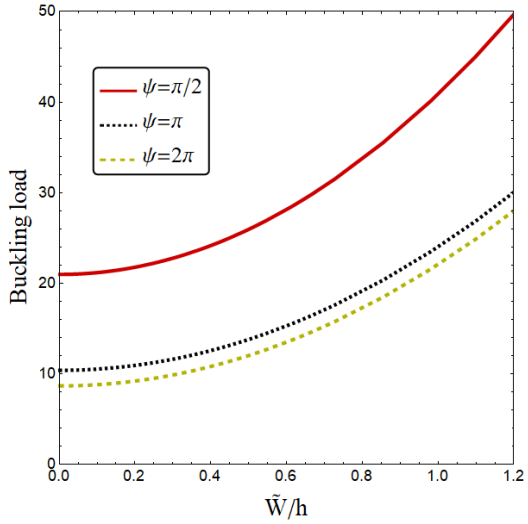

Fig. 5 Buckling load variation against non-dimensional amplitude of sandwich annular plate based on various sector angle ($W_{particle}$=0.4%, h_f=0.2h, r_0=0.2r_1, t=0.01l)

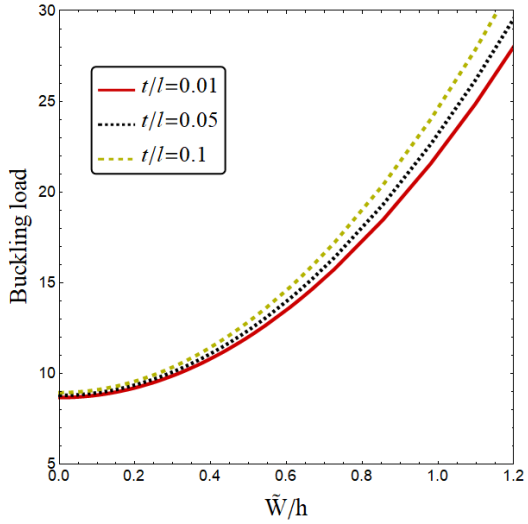

Fig. 6 Buckling load variation against non-dimensional amplitude of sandwich annular plate based on various honeycomb wall thickness ($W_{particle}$=0.4%, h_f=0.2h, r_0=0.2r_1, t=0.01l)

Buckling load of GOP reinforced annular sector sandwich plate versus dimensionless deflection for different sector angle has been shown in Fig. 5. The figure shows that higher values for sector angle result in lower post-buckling loads. This is because the annular sectorial sandwich plate is more stiff at lower values of sector angle. Thus, the minimum value of buckling load has been obtained for a complete annular sandwich plate.

In Fig. 6, post-buckling load-amplitude curves of a particle-reinforced annular sandwich plate have been presented accounting for various honeycomb core wall thickness (t/l). The most important observation from this figure is that a higher value of honeycomb core wall thickness gives greater buckling loads. Such observation is due to the reason that with the growth of honeycomb core wall thickness, the core layer becomes stiffer leading to a higher total stiffness of the annular sandwich plate. Thus, the buckling load of the annular sandwich plate can be enhanced via increasing the thickness of core walls.

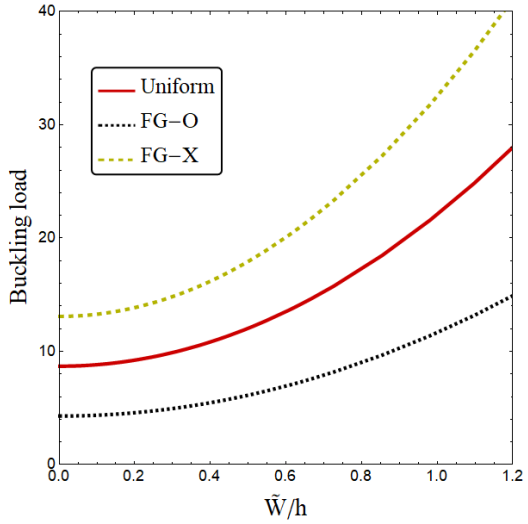

Fig. 7 Buckling load variation against non-dimensional amplitude of sandwich annular plate based on various GOP dispersions ($W_{particle}$=0.4%, h_f=0.2h, r_0=0.2r_1, t=0.01l)

The particle dispersion effect on post-buckling behavior of annular sandwich plate has been illustrated in Fig. 7. Various dispersions including uniform dispersion and two graded dispersions (FG-O and FG-X) have been considered. The most significant observation from this figure is that FG-X type of particle dispersion gives greater post-buckling loads than uniform and FG-O dispersions. As an outcome, controlling of GOP particles within the layers is vital for obtaining the best mechanical performances of annular sandwich plates.

7. Conclusions

This article analyzed post-buckling behaviors of GOP-reinforced annular sandwich plates via stablishing a nonlinear annular plate formulation. Uniform and functionally graded GOP distributions were considered. Obtained findings in this research are presented as follows.

• Increasing GOP particle weight fraction yields larger buckling loads. It means that adding the amount of nanoparticle can increase the plate stiffness and enhance its post-buckling behavior.

• FG-X particle distribution provided greater post-buckling loads than other distributions.

• An important finding was that as the magnitude of sector angle is greater, the buckling load is lower.

• The buckling load of the annular sandwich plate can be enhanced via increasing the thickness of core walls

Funding

This work was supported by the second “Zhanlan Scholar Project” Funding Project of Dalian Ocean University

(191022007); 2020 Scientific Research Fund Project of Liaoning Education Department (QL202017); 2019 Science and Technology Fund project of Liaoning Province (BS-201933); Funded by the Dalian Ocean University Innovation team (C202114).

References

Afshari, B.M., Mirjavadi, S.S. and Barati, M.R. (2022), "Investigating nonlinear static behavior of hyperelastic plates using three-parameter hyperelastic model", *Adv. Concr. Constr.*, **13**(5), 377-384. https://doi.org/10.12989/acc.2022.13.5.377.

Ahankari, S.S. and Kar, K.K. (2010), "Hysteresis measurements and dynamic mechanical characterization of functionally graded natural rubber–carbon black composites", *Polym. Eng. Sci.*, **50**(5), 871-877. https://doi.org/10.1002/pen.21601.

Al-Maliki, A.F., Faleh, N.M. and Alasadi, A.A. (2019), "Finite element formulation and vibration of nonlocal refined metal foam beams with symmetric and non-symmetric porosities", *Struct. Monit. Maint.*, **6**(2), 147-159. https:// doi.org/10.12989/smm.2019.6.2.147.

Barati, M.R. (2017a), "Nonlocal-strain gradient forced vibration analysis of metal foam nanoplates with uniform and graded porosities", *Adv. Nano Res.*, **5**(4), 393-414. https://doi.org/10.12989/anr.2017.5.4.393.

Barati, M.R. (2017b), "Vibration analysis of multi-phase nanocrystalline material nanoshells using strain gradient elasticity", *Mater. Res. Express*, **4**(10), 105021. https://doi.org/10.1088/2053-1591/aa89fb.

Barati, M.R. and Shahverdi, H. (2017a), "Dynamic modeling and vibration analysis of double-layered multi-phase porous nanocrystalline silicon nanoplate systems", *Eur. J. Mech. A Solids*, **66**, 256-268. https://doi.org/10.1016/j.euromechsol.2017.07.010.

Barati, M.R. and Shahverdi, H. (2017b), "Frequency analysis of porous nano-mechanical mass sensors made of multi-phase nanocrystalline silicon materials", *Mater. Res. Express*, **4**(7), 075019. https://doi.org/10.1088/2053-1591/aa7ac2.

Barati, M.R. and Shahverdi, H. (2022), "Vibration frequencies of meta-material plates based on the numerical calibration of shape factor for various cell patterns", *Waves Random Complex Med.*, 1-19. https://doi.org/10.1080/17455030.2022.2046300.

Barati, M.R. and Zenkour, A.M. (2018), "Analysis of postbuckling of graded porous GPL-reinforced beams with geometrical imperfection", *Mech. Adv. Mater. Struct.*, **26**(6), 503-511. https://doi.org/10.1080/15376494.2017.1400622.

Barati, M.R. and Zenkour, A. (2019), "Investigating instability regions of harmonically loaded refined shear deformable inhomogeneous nanoplates", *Iranian J. Sci. Technol. Transact. Mech. Eng.*, **43**(3), 393-404. https://doi.org/10.1007/s40997-018-0215-4.

Chikh, A., Bakora, A., Heireche, H., Houari, M.S.A., Tounsi, A. and Bedia, E.A. (2016), "Thermo-mechanical postbuckling of symmetric S-FGM plates resting on Pasternak elastic foundations using hyperbolic shear deformation theory", *Struct. Eng. Mech.*, **57**(4), 617-639. https://doi.org/10.12989/sem.2016.57.4.617.

Du, H., Gao, H.J. and Dai Pang, S. (2016), "Improvement in concrete resistance against water and chloride ingress by adding graphene nanoplatelet", *Cement Concr. Res.*, **83**, 114-123. https://doi.org/10.1016/j.cemconres.2016.02.005.

Ebrahimi, F. and Barati, M.R. (2017a), "A third-order parabolic shear deformation beam theory for nonlocal vibration analysis of magneto-electro-elastic nanobeams embedded in two-parameter elastic foundation", *Adv. Nano Res.*, **5**(4), 313-336. https://doi.org/10.12989/anr.2017.5.4.313.

Ebrahimi, F. and Barati, M.R. (2017b), "A general higher-order nonlocal couple stress based beam model for vibration analysis of porous nanocrystalline nanobeams", *Superlattice Microst.*, **112**, 64-78. https://doi.org/10.1016/j.spmi.2017.09.010.

Ebrahimi, F. and Barati, M.R. (2017c), "Thermal-induced nonlocal vibration characteristics of heterogeneous beams", *Adv. Mater. Res.*, **6**(2), 93. https://doi.org/10.12989/amr.2017.6.2.093.

Ebrahimi, F. and Barati, M.R. (2017d), "Buckling analysis of nonlocal embedded shear deformable functionally graded piezoelectric nanoscale beams", *Jordan J. Mech. Ind. Eng.*, **11**(2).

Ebrahimi, F. and Barati, M.R. (2017e), "Vibration analysis of heterogeneous nonlocal beams in thermal environment", *Coupled Syst. Mech.*, **6**(3), 251-272. https://doi.org/10.12989/csm.2017.6.3.251.

Ebrahimi, F. and Barati, M.R. (2018a), "Static stability analysis of double-layer graphene sheet system in hygro-thermal environment", *Microsyst. Technol.*, **24**(9), 3713-3727. https://doi.org/10.1007/s00542-018-3827-0.

Ebrahimi, F. and Barati, M.R. (2018b), "Influence of neutral surface position on dynamic characteristics of in-homogeneous piezo-magnetically actuated nanoscale plates", *Proceedings of the Institution of Mechanical Engineers, Part C: Journal of Mechanical Engineering Science*, **232**(17), 3125-3143. https://doi.org/10.1177/0954406217728977.

Ebrahimi, F. and Barati, M.R. (2018c), "A nonlocal strain gradient refined plate model for thermal vibration analysis of embedded graphene sheets via DQM", *Struct. Eng. Mech.*, **66**(6), 693-701. https://doi.org/10.12989/sem.2018.66.6.693.

Ebrahimi, F. and Barati, M. R. (2018d), "A unified formulation for modeling of inhomogeneous nonlocal beams", *Struct. Eng. Mech.*, **66**(3), 369-377. https://doi.org/10.12989/sem.2018.66.3.369.

Ebrahimi, F. and Barati, M.R. (2018e), "Thermo-mechanical vibration analysis of nonlocal flexoelectric/piezoelectric beams incorporating surface effects", *Struct. Eng. Mech.*, **65**(4), 435-445. https://doi.org/10.12989/sem.2018.65.4.435.

Ebrahimi, F. and Barati, M.R. (2018f), "Size-dependent thermally affected wave propagation analysis in nonlocal strain gradient functionally graded nanoplates via a quasi-3D plate theory", *Proceedings of the Institution of Mechanical Engineers, Part C: Journal of Mechanical Engineering Science*, **232**(1), 162-173. https://doi.org/10.1177/0954406216674243.

Ebrahimi, F. and Barati, M.R. (2019a), "Buckling characteristics of bilayer graphene sheets subjected to humid thermo-mechanical loading", *Handbook Graphene*, **8**, 433.

Ebrahimi, F. and Barati, M.R. (2019b), "On static stability of electro-magnetically affected smart magneto-electro-elastic nanoplates", *Adv. Nano Res.*, **7**(1), 63-76. https://doi.org/10.12989/anr.2019.7.1.063.

Ebrahimi, F., Barati, M.R. and Mahesh, V. (2019), "Dynamic modeling of smart magneto-electro-elastic curved nanobeams", *Adv. Nano Res.*, **7**(3), 145-155. https://doi.org/10.12989/anr.2019.7.3.145.

Ebrahimi, F., Barati, M.R. and Tornabene, F. (2019), "Mechanics of nonlocal advanced magneto-electro-viscoelastic plates", *Struct. Eng. Mech.*, **71**(3), 257-269. https://doi.org/10.12989/sem.2019.71.3.257.

Esawi, A. M.K., Morsi, K., Sayed, A., Taher, M. and Lanka, S. (2011), "The influence of carbon nanotube (CNT) morphology and diameter on the processing and properties of CNT-reinforced aluminium composites", *Compos. Part A*, **42**(3), 234-243.

Fang, M., Wang, K., Lu, H., Yang, Y. and Nutt, S. (2009),

"Covalent polymer functionalization of graphene nanosheets and mechanical properties of composites," *J. Mater. Chem.*, **19**(38), 7098-7105. https://doi.org/10.1039/B908220D.

Fenjan, R.M., Ahmed, R.A., Alasadi, A.A. and Faleh, N.M. (2019), "Nonlocal strain gradient thermal vibration analysis of double-coupled metal foam plate system with uniform and non-uniform porosities", *Coupled Syst. Mech.*, **8**(3), 247-257. https://doi.org/10.12989/csm.2019.8.3.247.

Feng, C., Kitipornchai, S. and Yang, J. (2017), "Nonlinear free vibration of functionally graded polymer composite beams reinforced with graphene nanoplatelets (GPLs)", *Eng. Struct.*, **140**, 110-119. https://doi.org/10.1016/j.engstruct.2017.02.052.

Gojny, F.H., Wichmann, M.H.G., Köpke, U., Fiedler, B and Schulte, K. (2004), "Carbon nanotube-reinforced epoxy-composites: enhanced stiffness and fracture toughness at low nanotube content", *Compos. Sci. Technol.*, **64**(15), 2363-2371. https://doi.org/10.1016/j.compscitech.2004.04.002.

Guan, H., Huang, S., Ding, J., Tian, F., Xu, Q. and Zhao, J. (2020), "Chemical environment and magnetic moment effects on point defect formations in CoCrNi-based concentrated solid-solution alloys," *Acta Materialia*, **187**, 122-134. https://doi.org/10.1016/j.actamat.2020.01.044.

Guenaneche, B., Benyoucef, S., Tounsi, A. and Adda Bedia, E. A. (2019), "Improved analytical method for adhesive stresses in plated beam: Effect of shear deformation," *Adv. Concr. Constr.*, **7**(3), 151-166. https://doi.org/10.12989/acc.2019.7.3.151.

Hao, P., Wang, B., Du, K., Li, G., Tian, K., Sun, Y. and Ma, Y. (2016), "Imperfection-insensitive design of stiffened conical shells based on equivalent multiple perturbation load approach," *Compos. Struct.*, **136**, 405-413. https://doi.org/10.1016/j.compstruct.2015.10.022.

Hao, R.B., Lu, Z.Q., Ding, H. and Chen, L.Q. (2022), "A nonlinear vibration isolator supported on a flexible plate: analysis and experiment," *Nonlinear Dynamics*, **108**(2), 941-958. https://doi.org/10.1007/s11071-022-07243-7.

King, J.A., Klimek, D.R., Miskioglu, I. and Odegard, G.M. (2013), "Mechanical properties of graphene nanoplatelet/epoxy composites," *J. Appl. Polym. Sci.*, **128**(6), 4217-4223. https://doi.org/10.1002/app.38645.

Kitipornchai, S., Chen, D. and Yang, J. (2017), "Free vibration and elastic buckling of functionally graded porous beams reinforced by graphene platelets," *Mater. Des.*, **116**, 656-665. https://doi.org/10.1016/j.matdes.2016.12.061.

Lal, A. and Markad, K. (2018), "Deflection and stress behaviour of multi-walled carbon nanotube reinforced laminated composite beams", *Comput. Concr.*, **22**(6), 501-514. https://doi.org/10.12989/cac.2018.22.6.501.

Liew, K.M., Lei, Z.X. and Zhang, L.W. (2015), "Mechanical analysis of functionally graded carbon nanotube reinforced composites: A review", *Compos. Struct.*, **120**, 90-97. https://doi.org/10.1016/j.compstruct.2014.09.041.

Lin, F., Yang, C., Zeng, Q.H. and Xiang, Y. (2018), "Morphological and mechanical properties of graphene-reinforced PMMA nanocomposites using a multiscale analysis", *Comput. Mater. Sci.*, **150**, 107-120.

Liu, W., Huang, F., Liao, Y., Zhang, J., Ren, G., Zhuang, Z. and Wang, C. (2008), "Treatment of CrVI-Containing Mg (OH) 2 Nanowaste," *Angewandte Chemie*, **120**(30), 5701-5704. https://doi.org/10.1002/ange.200800172.

Metwally, I.M. (2014), "Three-dimensional finite element analysis of reinforced concrete slabs strengthened with epoxy-bonded steel plates", *Adv. Concr. Constr.*, **2**(2), 91. https://doi.org/10.12989/acc.2014.2.2.091.

Mirjavadi, S.S., Khan, I., Forsat, M., Barati, M.R. and Hamouda, A.M.S. (2020a)," Analyzing nonlinear vibration of metal foam stiffened toroidal convex/concave shell segments considering porosity distribution," *Mech. Based Des. Struct.*, 1-17. https://doi.org/10.1080/15397734.2020.1841654.

Mirjavadi, S.S., Yahya, Y.Z., Forsat, M., Khan, I., Hamouda, A.M.S. and Barati, M.R. (2020b)," Magneto-electric effects on nonlocal nonlinear dynamic characteristics of imperfect multi-phase magneto-electro-elastic beams," *J. Magnet. Magnet. Mater.*, **503**, 166649. https://doi.org/10.1016/j.jmmm.2020.166649.

Mirjavadi, S.S., Bayani, H., Khoshtinat, N., Forsat, M., Barati, M.R. and Hamouda, A.M.S. (2020c), "On nonlinear vibration behavior of piezo-magnetic doubly-curved nanoshells," *Smart Struct. Syst.*, **26**(5), 631-640. https://doi.org/10.12989/sss.2020.26.5.631.

Mirjavadi, S.S., Forsat, M., Barati, M.R. and Hamouda, A. M.S. (2020d), "Nonlinear forced vibrations of multi-scale epoxy/ CNT/fiberglass truncated conical shells and annular plates via 3D Mori-Tanaka scheme," *Steel Compos. Struct.*, **35**(6), 765-777. https://doi.org/10.12989/scs.2020.35.6.765.

Mirjavadi, S.S., Forsat, M., Yahya, Y.Z., Barati, M.R., Jayasimha, A.N. and Khan, I. (2020e), "Finite element based post-buckling analysis of refined graphene oxide reinforced concrete beams with geometrical imperfection", *Comput. Concr.*, **25**(4), 283-291. https://doi.org/10.12989/cac.2020.25.4.283.

Mirjavadi, S.S., Forsat, M., Barati, M.R. and Hamouda, A. M.S. (2021), "Investigating nonlinear vibrations of multi-scale truncated conical shell segments with carbon nanotube/ fiberglass reinforcement using a higher order conical shell theory", *J. Strain Anal. Eng. Des.*, **56**(3), 181-192. https://doi.org/10.1177/0309324720939811.

Mirjavadi, S.S., Forsat, M., Barati, M.R. and Hamouda, A. S. (2022), "Nonlinear vibrations of variable thickness curved panels made of multi-scale epoxy/fiberglass/CNT material using Jacobi elliptic functions", *Mech. Based Des. Struct.*, **50**(7), 2333-2349. https://doi.org/10.1080/15397734.2020.1777156.

Mohammed, A., Sanjayan, J.G., Nazari, A. and Al-Saadi, N.T.K. (2017), "Effects of graphene oxide in enhancing the performance of concrete exposed to high-temperature", *Aust. J. Civil Eng.*, **15**(1), 61-71. https://doi.org/10.1080/14488353.2017.1372849.

Nieto, A., Bisht, A., Lahiri, D., Zhang, C and Agarwal, A. (2017), "Graphene reinforced metal and ceramic matrix composites: A review", *Int. Mater. Rev.*, **62**(5), 241-302. https://doi.org/10.1080/09506608.2016.1219481.

Rafiee, M.A., Rafiee, J., Wang, Z., Song, H., Yu, Z.Z. and Koratkar, N. (2009), "Enhanced mechanical properties of nanocomposites at low graphene content", *ACS nano*, **3**(12), 3884-3890. https://doi.org/10.1021/nn9010472.

Rezaiee-Pajand, M., Masoodi, A.R. and Mokhtari, M. (2018), "Static analysis of functionally graded non-prismatic sandwich beams", *Adv. Comput. Des.*, **3**(2), 165-190. https://doi.org/10.12989/acd.2018.3.2.165.

Shamsaei, E., de Souza, F.B., Yao, X., Benhelal, E., Akbari, A. and Duan, W. (2018), "Graphene-based nanosheets for stronger and more durable concrete: A review", *Constr. Build. Mater.*, **183**, 642-660. https://doi.org/10.1016/j.conbuildmat.2018.06.201.

Shen, H.S., Xiang, Y., Lin, F. and Hui, D. (2017). Buckling and postbuckling of functionally graded graphene-reinforced composite laminated plates in thermal environments", *Compos. Part B Eng.*, **119**, 67-78. https://doi.org/10.1016/j.compositesb.2017.03.020.

Song, M., Kitipornchai, S. and Yang, J. (2017), "Free and forced vibrations of functionally graded polymer composite plates reinforced with graphene nanoplatelets," *Compos. Struct.*, **159**, 579-588. https://doi.org/10.1016/j.compstruct.2016.09.070.

Wang, L. and Su, R.K.L. (2013), "A unified design procedure for preloaded rectangular RC columns strengthened with post-compressed plates", *Adv. Concr. Constr.*, **1**(2), 163.

https://doi.org/10.12989/acc.2013.1.2.163.
Wang, B., Zhu, S., Hao, P., Bi, X., Du, K., Chen, B., and Chao, Y.J. (2018), "Buckling of quasi-perfect cylindrical shell under axial compression: A combined experimental and numerical investigation", *Int. J. Solids Struct.*, **130**, 232-247. https://doi.org/10.1016/j.ijsolstr.2017.09.029.
Wu, Y., Zhao, Y., Han, X., Jiang, G., Shi, J., Liu, P. and Yamada, Y. (2021), "Ultra-fast growth of cuprate superconducting films: Dual-phase liquid assisted epitaxy and strong flux pinning", *Mater. Today Phys.*, **18**, 100400. https://doi.org/10.1016/j.mtphys.2021.100400.
Xiong, Q.M., Chen, Z., Huang, J.T., Zhang, M., Song, H., Hou, X.F. and Feng, Z.J. (2020), "Preparation, structure and mechanical properties of Sialon ceramics by transition metal-catalyzed nitriding reaction", *Rare Metals*, **39**(5), 589-596. https://doi.org/10.1007/s12598-020-01385-6.
Yang, B., Yang, J. and Kitipornchai, S. (2017), "Thermoelastic analysis of functionally graded graphene reinforced rectangular plates based on 3D elasticity", *Meccanica*, **52**(10), 2275-2292. https://doi.org/10.1007/s11012-016-0579-8.
Zaheer, M.M., Jafri, M.S. and Sharma, R. (2019), "Effect of diameter of MWCNT reinforcements on the mechanical properties of cement composites", *Adv. Concr. Constr.*, **8**(3), 207-215. https://doi.org/10.12989/acc.2019.8.3.207.
Zhang, L.W. (2017), "On the study of the effect of in-plane forces on the frequency parameters of CNT-reinforced composite skew plates", *Compos. Struct.*, **160**, 824-837. https://doi.org/10.1016/j.compstruct.2016.10.116.
Zhang, Z., Li, Y., Wu, H., Zhang, H., Wu, H., Jiang, S. and Chai, G. (2020), "Mechanical analysis of functionally graded graphene oxide-reinforced composite beams based on the first-order shear deformation theory", *Mech. Adv. Mater. Struct.*, **27**, 3-11. https://doi.org/10.1080/15376494.2018.1444216.

CC